11-2013

Melt Inclusion Evidence for Magma Evolution at Mutnovsky Volcano, Kamchatka

K. Robertson

A. Simon

T. Pettke

Sean R. Mulcahy
Western Washington University, sean.mulcahy@wwu.edu

E. Smith

See next page for additional authors

GEOFLUIDS

Geofluids (2013) **13**, 421–439 doi: 10.1111/gfl.12060

Melt inclusion evidence for magma evolution at Mutnovsky volcano, Kamchatka

K. ROBERTSON[1], A. SIMON[2], T. PETTKE[3], E. SMITH[1], O. SELYANGIN[4], A. KIRYUKHIN[5], S. R. MULCAHY[6] AND J. D. WALKER[7]

[1]Department of Geoscience, University of Nevada Las Vegas, Las Vegas, NV, USA; [2]Department of Earth and Environmental Sciences, University of Michigan, Ann Arbor, MI, USA; [3]Institute of Geological Sciences, University of Bern, Bern, Switzerland; [4]Research Geotechnological Center, Far Eastern Division, Russian Academy of Sciences, Petropavlovsk-Kamchatsky, Russia; [5]Institute of Volcanology and Seismology Far East Branch, Russian Academy of Sciences, Petropavlovsk-Kamchatsky, Russia; [6]Department of Earth and Planetary Science, University of California Berkeley, Berkeley, CA, USA; [7]Department of Geology, University of Kansas, Lawrence, KS, USA

ABSTRACT

Mutnovsky Volcano, located in Kamchatka, Russia, is a young volcano that has formed a series of four overlapping stratocones over its approximately 80 ka history. Erupted products at Mutnovsky range in composition from basalts to dacites; basalts are the most common. In this study, melt inclusions from representative samples of all erupted compositions from all four eruptive centers were analyzed to investigate the causes of the compositional heterogeneity, melt evolution, and pre-eruptive magma dynamics. Melt inclusions from Mutnovsky were sampled in olivine, plagioclase, orthopyroxene, and clinopyroxene. The melt inclusion data represent a wide range of melt compositions, from basalt through rhyolite. Geochemical modeling of melt inclusion data, combined with field evidence and chemical zoning of plagioclase phenocrysts, indicates that fractional crystallization and magma mixing produced the range of erupted bulk rock compositions. The measured variability of melt inclusion compositions in each host mineral phase indicates that different host minerals trapped unique melts that evolved separately from one another. The melt inclusion data suggest that individual melt portions evolved by fractional crystallization, perhaps in different magma chambers, within the Mutnovsky plumbing system, and were mixed prior to eruption. Our data do not indicate whether the mixing events were the cause of eruption or are simply the manifestation of the eruption process.

Key words: amphibole sponge, fractional crystallization, magma mixing, melt inclusion, partial melt, slab input, underplated basalt, volcano

Received 11 August 2012; accepted 26 July 2013

Corresponding author: Adam Simon, Department of Earth and Environmental Sciences, University of Michigan, 2534 C.C. Little Building, 1100 N. University Avenue, Ann Arbor, MI 48109-1005, USA.
Email: simonac@umich.edu. Tel: +734 647 4245. Fax: +734 763 4690.

Geofluids (2013) **13**, 421–439

INTRODUCTION

Arc volcanoes provide geochemical insight into the nature of material transfer from ocean lithosphere and overlying meta-sediments to the mantle and crust during subduction, hence placing constraints on the cycling of material among mantle, crust, and atmosphere (Manning 2004). The fundamental geologic processes that result in the formation of arc-related volcanic rocks, from partial melting of the mantle wedge above subducting ocean lithosphere to degassing-induced eruption, have been relatively well constrained through a combined approach of field, laboratory, and computational efforts (Putirka & Tepley 2008). What is lacking, however, is a general consensus on the specific causes of compositional diversity (i.e., heterogeneity) observed among magmas erupted from individual volcanoes. For example, it seems well recognized that composite stratovolcanoes in continental arcs commonly erupt magmas that are volumetrically dominated by one bulk composition. That is, erupting dominantly basalt, andesite, dacite, or rhyolite. However, the observation that arc volcanoes commonly erupt a range of compositions has stimulated efforts to constrain the origin of these compositional variations. A number of hypotheses have been put forth to

explain the eruption of compositionally diverse magmas from individual volcanoes, that is, volcanoes erupted within individual arc segments and volcanoes in distinct arc settings (Plank & Langmuir 1988). These include formation and ascent of unique aliquots of magma in the mantle, each produced by variable degrees of partial melting from of the mantle (Bacon *et al.* 1997), variable extents of mixing, assimilation, storage, and homogenization of magmas at the base of variably thickened crust (Leeman,1983; Hildreth & Moorbath 1988; Annen *et al.* 2006), physical and chemical mixing of magmas in mid- to upper-crustal magma chambers (Kent *et al.* 2010), and variable contributions from direct melting of the subducted slab (e.g., Kay 1978; Defant & Drummond 1990; Yogodzinski *et al.* 1995; Bryant *et al.* 2010).

Historically, a major challenge to investigating the compositional variability of magmas erupted from individual volcanoes arose from the fact that one could sample only the solidified end products of arc volcanism. That is, the pre-eruptive silicate melt portion was accessible only for magmas that erupted largely in their liquid state and quenched to a glass. Over the past few decades, the recognition that aliquots of silicate liquid are trapped as melt inclusions in growing crystals has facilitated acquisition of data that provide insight into the compositional variability of silicate melts within and among individual erupted magmas (Anderson 1976; Kent 2010). As such, melt inclusions have become an increasingly important tool for improving our understanding of the magmatic processes responsible for compositional diversity among erupted magmas. Melt inclusions provide much more detailed samples of melt compositions than we can gain with whole-rock analyses alone. The chemical composition of melt inclusions demonstrate that melts within individual volcanic systems are much more diverse than originally thought (e.g., Charlier *et al.* 2007), that magma mixing in near-surface magma chambers may be an important source of compositional change and eruption triggering (Kent *et al.* 2010 and references therein), and that there can be multiple populations of compositionally distinct melts present within one volcanic system (Halter *et al.* 2004a). Melt inclusions also provide the best possibility to determine quantitatively the pre-eruptive volatile contents of melts, and how these are related to degassing and eruption processes (Blundy & Cashman 2005; Wallace 2005; Métrich & Wallace 2008).

In this study, we take advantage of melt inclusions to explore the compositional diversity among erupted magmas from Mutnovsky Volcano, Kamchatka, a volcano in a young, continental arc, which has erupted basalt, basaltic andesite, andesite, and dacite. Mutnovsky is volumetrically dominated by basalt and basaltic andesite, and discrete eruptions of intermediate to felsic magmas have erupted over the approximately 80 ka life of the volcano (Selyangin 1993). We quantified the major, minor, and trace element chemistry, not including volatiles, of 215 melt inclusions from 15 different whole-rock samples representing the complete whole-rock compositional spectrum from Mutnovsky. The measured Nd, Sr, and Pb isotope abundances for the whole-rock samples ($^{143}Nd/^{144}Nd$ ranges from 0.513060 to 0.513083, $^{87}Sr/^{86}Sr$ ranges from 0.703335 to 0.703387 ^{206}, $Pb/^{204}Pb$ ranges from 18.315 to 18.361, and $^{207}Pb/^{204}Pb$ ranges from 15.468 to 15.497) demonstrate that the magmas are not affected by assimilation of exotic material, and all share a common source. This obviates the need to back out compositional changes introduced by assimilation of rocks external to the magma plumbing system.

The melt inclusion data provide information about compositionally discrete melt populations, how the different melt populations relate to progressive magma evolution, and how they are related to the phenocryst phases in Mutnovsky samples. The relationship of the melt inclusion compositions to whole-rock compositions elucidates the importance of magmatic differentiation processes such as fractional crystallization and magma mixing and improves our understanding of the origin of the diversity of igneous rocks.

GEOLOGICAL SETTING

Mutnovsky Volcano is a part of the Eastern Volcanic Front in southern Kamchatka, about 75 km southwest of Petropavlovsk-Kamchatsky (Fig. 1). Mutnovsky formed over the past 80 ka by eruptions related to four stratocones, referred to as Mutnovsky I, II, III, and IV. The eruptive centers have been placed in a relative time sequence, with Mutnovsky I the oldest and Mutnovsky IV the youngest, based on glacial deposits and tephrochronology. There are no radiogenic ages for Mutnovsky. The majority of the erupted products in all the stratocones are basalt and basaltic andesite; however, Mutnovsky I, II, and III also erupted andesite and dacite. A more detailed description of Mutnovsky's geologic setting is found in Robertson (2011) and Selyangin (1993, 2009).

SAMPLE SELECTION AND METHODS

This article focuses on the chemistry of melt inclusions from a subset of samples for which the whole-rock and mineral chemistry were described in detail in Robertson (2011). A total of 50 whole-rock samples were collected from across the eruptive centers Mutnovsky I (oldest) to IV (youngest). We petrographically characterized thin sections from all whole-rock samples and analyzed all whole-rock samples for major and trace element abundances (Robertson 2011). Whole-rock chemistry was performed by crushing, pulverizing, and then powdering with a steel disk mill a representative portion of each whole-rock

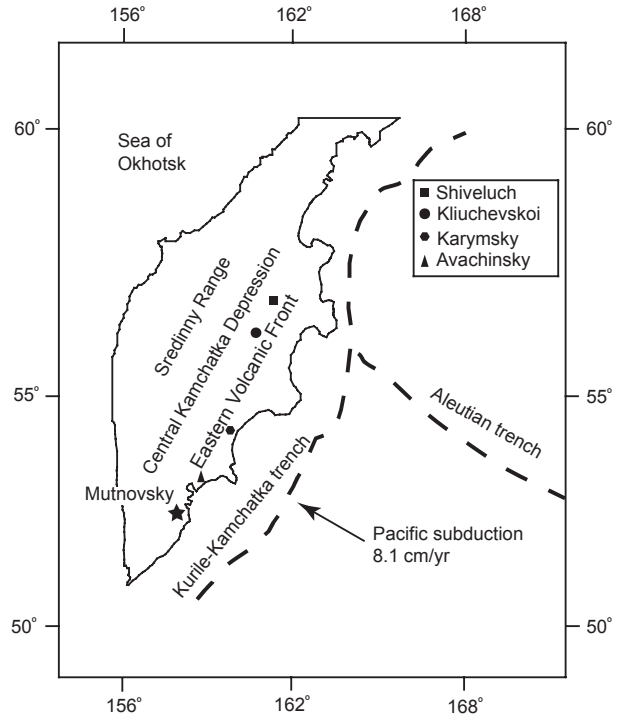

Fig. 1. Schematic map of the Kamchatka peninsula showing the location of subduction and major volcanic centers, including Mutnovsky. Subduction rate from Moore *et al.* (1992).

sample to ensure complete sample homogenization before geochemical analysis. Major and trace element abundances were quantified using inductively coupled plasma mass spectrometry (ICP-MS) on whole-rock powders at Activation Laboratories, Ltd. in Ontario, Canada. Major element abundances were determined using lithium metaborate/tetraborate fusion of rock powders and analysis on either a combination simultaneous/sequential Thermo-Jarrell-Ash ENVIRO II or a Varian Vista 735 ICP-MS. Trace element abundances were determined using lithium metaborate/tetraborate fusion of rock powders, which were analyzed by a Perkin Elmer Sciex ELAN 6000, 6100, or 9000 ICP-MS.

We used a JEOL JXA-8900 SuperProbe electron probe microanalyzer (EPMA) to quantify the compositions of plagioclase and pyroxene in all thin sections (Robertson 2011). Plagioclase analyses were performed with a 15 kV accelerating voltage, a 10 nA Faraday cup current, and a beam diameter of 5 μm for each spot. Line traverses were set up across plagioclase grains, from rim to rim, with 7 μm spacing between spots (from the center of one spot to the center of the next). Monte Carlo simulations of the energy distribution for these EPMA beam conditions indicate that >98% of the absorbed energy is retained within the 5 μm spot size. Pyroxene analyses were performed with a 15 kV accelerating voltage, a 10 nA Faraday cup current, and a beam diameter of 10 microns for most crystals. We used an appropriately sized beam for crystals measuring <10 microns in maximum diameter. Most pyroxene crystals were only large enough for one analysis per crystal, but two analyses, core and rim, were performed on crystals larger than approximately 20 microns. The larger crystals (i.e., >20 microns) displayed no measurable compositional zoning, based on core and rim analyses and back-scattered electron (BSE) imaging.

After petrographic characterization of thin sections for all whole-rock samples, we selected 15 samples for the purpose of our melt inclusion study. Four samples from Mutnovsky I, II, and III, and three samples from Mutnovsky IV were selected. The samples from Mutnovsky I, II, and III include a basalt, basaltic andesite, andesite, and dacite, and from Mutnovsky IV include two basalts and a basaltic andesite. In each case, samples were selected to represent the range of compositions present in each eruptive center and for containing the greatest number of petrographically discernible melt inclusions that met the criteria for LA-ICP-MS analysis, described below.

We prepared new, double polished 200 μm thick sections from each of the 15 selected whole-rock samples. Melt inclusions were selected from olivine, clinopyroxene, orthopyroxene, and plagioclase, which together constitute the major phenocryst phases among the Mutnovsky samples. The size of phenocrysts ranged from approximately 200 to approximately 3000 microns in diameter. Most melt inclusions were recrystallized, but some partially devitrified and purely glassy inclusions with a shrinkage bubble were also identified and analyzed (Fig. 2). Only those inclusions that measured ≥10 μm in diameter, located no deeper in their host mineral than the melt inclusion diameter (i.e., a 10 μm diameter inclusion was not deeper than ≤10 μm below the host mineral surface), and not exposed at the surface of the thick section were targeted for analysis, following principles outlined in Pettke (2006). Whenever possible, melt inclusion assemblages (Halter *et al.* 2004a,b; Bodnar & Student 2006) were analyzed to provide multiple samples of the same generation of melt, which is assumed to have been locally compositionally uniform at the time of inclusion assemblage formation. Care was taken to avoid melt inclusions with obvious signs of postentrapment modification such as alteration, leakage, or proximity to cracks and/or cleavage traces. Melt inclusions were not rehomogenized before analysis.

Entire, unexposed melt inclusions were analyzed using LA-ICP-MS at the University of Bern, Switzerland. The system is comprised of a GeoLas-Pro 193 nm ArF Excimer laser ablation system (Lambda Physik, Germany) combined with an Elan DRC-e quadrupole ICP-MS (Perkin Elmer, Canada). Individual melt inclusion transient signals were deconvolved from the host mineral signal using the procedure developed and described by Halter *et al.* (2002, 2004b) and reviewed and evaluated in Heinrich *et al.*

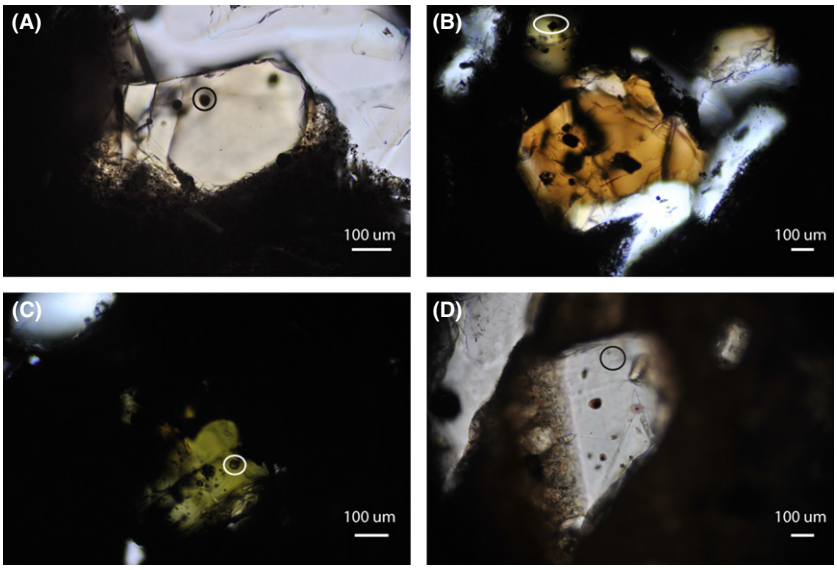

Fig. 2. Examples of recrystallized (A and B) and partially devitrified (C and D) melt inclusions in olivine (A), orthopyroxene (B), clinopyroxene (C), and plagioclase (D). Circles show the locations of melt inclusions analyzed in this study, which are not visible in the photographs in B and D. Other melt inclusions were not analyzed because they did not meet criteria for analysis (size, depth, quality).

(2003), Pettke *et al.* (2004, 2012), and Pettke (2006) through use of the Signal Integration for Laboratory Laser Systems (SILLS) program (Guillong *et al.* 2008). The data reduction strategy yields an uncertainty for each element of the analyte menu for each melt inclusion and host phenocryst, as described below.

Melt inclusion signal intervals were chosen manually for each inclusion by visually examining the entire major and trace element transient signal. Trace elements such as Zr, Y, and Ce provided the best evidence for distinguishing the melt inclusion portion of each transient signal relative to the phenocryst host (Fig. 3). Compositions of the host minerals and the mixed host plus inclusion signal intervals were quantified by summing to 100% oxides (Leach & Hieftje 2000; Halter *et al.* 2002). An internal standard is required to determine the analysis-specific mass fraction of

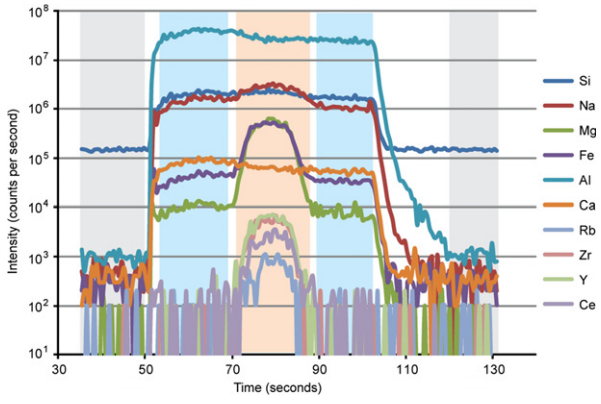

Fig. 3. Example of an LA-ICP-MS signal (melt inclusion 15mrb12 from sample CM-68). Areas shaded in gray are the gas background (which was collected from 0 to 50 sec and 120 to 150 sec), areas shaded in blue are the host mineral (plagioclase), and the area shaded in tan is the melt inclusion signal.

inclusion relative to host mineral in the mixed inclusion plus host signal interval of each LA-ICP-MS transient signal to calculate the pure melt inclusion composition. We comprehensively evaluated four data reduction approaches. Whole-rock values of K_2O and MnO were finally employed as internal standards: K_2O for olivine- and pyroxene-hosted melt inclusions and MnO for plagioclase-hosted melt inclusions. These elements were chosen because they are incompatible in the host minerals for which they were used. The data reduction approaches that we evaluated were (a) using whole-rock values of Al_2O_3 for all melt inclusions (e.g., Audétat and Pettke, 2003, who employed it for highly evolved systems); (b) using Al_2O_3 whole-rock values for olivine and pyroxene and MgO whole-rock values for plagioclase (e.g., Halter *et al.* 2002); (c) using Fe-Mg K_D values; and (d) using the fractionation trends method of Zajacz & Halter (2007). The results of each technique were evaluated for plausibility of major element concentrations, trace element ratios, and multiple K_D mineral-melt values (Fe-Mg in olivine, Mg in olivine, Ni in olivine, K in plagioclase, and Mn in pyroxene).

Melt inclusion compositions calculated using both whole-rock Al_2O_3 values and Al_2O_3 and MgO values (approaches a and b) as an internal standard yielded high total oxides (i.e., >102 wt.%) and often yielded implausible values for major elements, such as SiO_2, in the hundreds of wt.% range. Olivine Fe-Mg K_D values (approach c) were used to calculate an internal standard for melt inclusions hosted in olivine. The Fe/Mg ratio of each melt inclusion was determined using the Fe/Mg ratio of the host olivine and a K_D value of 0.31, which was calibrated experimentally for basalts at low pressures (0.1–0.3 GPa; Ulmer 1989). Melt inclusion compositions calculated using these K_D-determined internal standards were implausibly enriched in Al_2O_3, that is, >60 wt.%, Al_2O_3. The fraction-

ation method of Zajacz & Halter (2007) (approach d) is based on the assumption that the melt inclusions trapped a range of compositions along a liquid line of descent. In this method, the mass fraction (x) of melt inclusion relative to the host phenocryst phase is determined by the intersection of the regression line describing the liquid line of decent whole-rock values and the trend of progressive subtraction of the host mineral from the mixed signal of host plus melt inclusion. Incompatible versus compatible elements, in this case, FeO versus Al_2O_3 and CaO versus MgO, are plotted to form regression lines. These two sets of elements were chosen for comparison, and in each case, there was a compatible and incompatible element for each phenocryst phase. For both element pairs, the melt inclusion compositions calculated with the fractionation method often yielded calculated K_D values that were much higher or lower than experimentally determined published values. We suspect that the failure of employing major elements as the internal standard for melt inclusion plus host signal deconvolution may result from postentrapment partial re-equilibration of melt inclusion contents with host phenocrysts or even surrounding melt (for detailed discussions see e.g., Danyushevsky *et al.* 2002; Schiano 2003; Pettke 2006).

For all melt inclusion samples, the whole-rock K_2O and MnO incompatible element method consistently yielded calculated values in terms of oxide totals that are 99–102 wt.% and simultaneously yielded olivine Fe-Mg K_D values within approximately 10% of published values.

MELT INCLUSION AND HOST PHENOCRYST DATA

Table 1 contains the rock type, eruptive center, mineral assemblage, major element, and Nd, Sr, Pb, and isotope data for the 15 whole-rock samples analyzed during this study. Also presented are the latitude and longitude coordinates for samples where this information is known. Table 2 is presented as an online spreadsheet that contains the chemical data (major, minor, trace elements) for whole rocks, melt inclusions, and melt inclusion–host phenocrysts for 215 melt inclusion and 215 host phenocryst samples analyzed during this study. Each melt inclusion and its host phenocryst were ablated together and compositionally deconvolved as described above. Each individual laser ablation analysis yielded the chemical composition of the targeted melt inclusion and the surrounding host phenocryst. Thus, in Table 2, there is one analysis number for a melt inclusion (e.g., 17mrb06) and that specific melt inclusion host phenocryst (e.g., 17mrb06). Each set of melt inclusion and host phenocryst analyses is listed in Table 2 below their respective whole-rock sample number, and the eruptive center is indicated in parentheses following the whole-rock sample number. Also presented in Table 2 is the specific isotope measured for each element. The chemical data for all melt inclusions are grouped together, as are the data for the host phenocryst minerals. The compositional data for samples from Mutnovsky I are followed by data from Mutnovsky II, then Mutnovsky III, and finally Mutnovsky IV.

Table 1 Whole-rock major element, and Nd, Sr, and Pb isotope data for Mutnovsky samples. Major element data are in weight percent and trace element data are in parts per million (ppm).

Eruptive center	MI	MI	MI	MI	MII	MII	MII	MII
Sample	CM-97a	CM-5	M1-02-08	CM-47	CM-156	CM-142	CM-155	CM-113
Location			N 52.469117° E 158.16235°					
Rock Type	Basalt	Basaltic And.	Andesite	Dacite	Basalt	Basaltic And.	Andesite	Rhyodacite
Mineralogy	P, Ol, Opx, Cpx	P, Opx, Cpx	P, Opx, Cpx	P, Opx, Cpx	P, Ol, Opx, Cpx	P, Ol, Opx, Cpx	P, Opx	P, Opx
$^{143}Nd/^{144}Nd$	0.513108			0.513060	0.513089			0.513077
$^{87}Sr/^{86}Sr$	0.703387			0.703380	0.703355			0.703358
$^{206}Pb/^{204}Pb$	18.32			18.32	18.35			18.33
$^{207}Pb/^{204}Pb$	15.47			15.47	15.49			15.47
$^{208}Pb/^{204}Pb$	38.02			38.01	38.08			38.03
Mg#	0.56	0.44	0.36	0.35	0.55	0.42	0.34	0.28
SiO_2	50.52	52.38	58.71	64.68	48.68	53.44	57.27	67.53
Al_2O_3	17.75	18.18	16.48	16.04	18.65	17.33	15.73	14.63
FeO (T)	9.83	8.91	6.87	5.34	9.51	9.29	9.35	4.72
MnO	0.16	0.16	0.154	0.15	0.3	0.23	0.21	0.108
MgO	7.16	3.88	2.21	1.62	6.4	3.8	2.65	1.05
CaO	8.62	8.36	5.56	4.02	10.82	8.14	5.94	3.31
Na_2O	2.41	3.08	3.79	3.76	2.09	3.49	3.88	4.55
K_2O	0.54	0.72	1.24	1.98	0.48	0.72	1.3	2.1
TiO_2	1.09	1.18	0.91	0.91	1.17	1.31	1.45	0.47
P_2O_5	0.13	0.24	0.26	0.22	0.15	0.28	0.34	0.1
LOI	0.96	1.46	2.81	0.85	0.93	0.49	0.97	0.21
Total	100.29	99.54	99.74	100.16	100.24	99.55	100.13	99.33

P, plagioclase; Ol, olivine; Opx, orthopyroxene; Cpx, clinopyroxene.

Table 2 Electronic Supplement is presented as an online spreadsheet that contains chemical data (major, minor, trace elements) for whole rocks, melt inclusions, and melt inclusion–host phenocrysts for 215 melt inclusion and 215 host phenocryst samples analyzed during this study. The chemical data for samples from Mutnovsky I are followed by data from Mutnovsky II, then Mutnovsky III, and finally Mutnovsky IV. The chemical data for all melt inclusions are grouped together in rows A28–A254, as are the data for the host phenocryst minerals in rows A256–A481. Melt inclusions and their host phenocryst were ablated together and deconvolved. Each laser ablation analysis yielded the chemical composition of a melt inclusion and the surrounding host phenocryst. The uncertainty for each melt inclusion and separately for each host phenocryst is reported for each analyze. Thus, in Table 2, there is one analysis number for a melt inclusion (e.g., 17mrb06) and that specific melt inclusion host phenocryst (e.g., 17mrb06).

Eruptive center	MIII	MIII	MIII	MIII	MIV	MIV	MIV
Sample	M3-08-08	CM-9a	M3-09-08	CM-8a	CM-206	CM-68	CM-62
Location	N 52.4601° E158.161583°		N 52.463417° E158.167617°				
Rock Type	Basalt	Basaltic And.	Andesite	Dacite	Basalt	Basalt	Basaltic And.
Mineralogy	P, Ol, Cpx	P, Ol, Cpx	P, Opx, Cpx	P, Opx, Cpx	P, Ol, Opx, Cpx	P, Ol	P, Ol, Cpx
$^{143}Nd/^{144}Nd$	0.513101			0.513083		0.513079	0.513077
$^{87}Sr/^{86}Sr$	0.703335			0.703342		0.703346	0.703340
$^{206}Pb/^{204}Pb$	18.35			18.32		18.36	18.33
$^{207}Pb/^{204}Pb$	15.48			15.47		15.50	15.50
$^{208}Pb/^{204}Pb$	38.07			38.02		38.11	38.08
Mg#	0.52	0.55	0.37	0.27	0.51	0.54	0.51
SiO_2	48.85	52.8	58.83	69.4	51.08	50.46	54.02
Al_2O_3	22.65	19	18.01	14.61	18	20.74	17.37
FeO (T)	7.14	7.82	6.55	3.65	9.11	7.86	8.63
MnO	0.131	0.14	0.126	0.1	0.2	0.18	0.15
MgO	4.4	5.38	2.16	0.75	5.3	5.1	5
CaO	12.42	9.18	7.23	3.09	10.22	11.06	8.95
Na_2O	2.16	2.49	3.65	4.18	2.5	2.23	3.09
K_2O	0.28	0.66	1.62	3.18	0.6	0.54	1.2
TiO_2	0.59	0.79	0.84	0.63	1.11	0.77	1
P_2O_5	0.09	0.15	0.21	0.12	0.17	0.1	0.18
LOI	0.63	0.81	0.71	0.26	1.1	0.84	0.25
Total	100.1	100.09	100.7	100.33	100.4	100.14	100.09

Melt inclusion and phenocryst host uncertainties

The uncertainty for each element of the analyte menu was calculated individually for each melt inclusion and melt inclusion host phenocryst. These data are reported in Table 2. The average uncertainty and range of uncertainties for major, minor, and trace elements in melt inclusions and host phenocrysts are statistically small relative to the measured concentrations for each analyte. For example, the range of uncertainties for plagioclase-hosted melt inclusions varies as follows: SiO_2: 0.21–3.65 wt.%; Al_2O_3: range 0.20–3.14 wt.%; TiO_2: 0.004–0.915; FeO: 0.03–2.07 wt.%; MnO: 0.001–0.87 wt.%; MgO: 0.01–3.64 wt.%; CaO: 0.64–3.59 wt.%; Na_2O: 0.011–1.33 wt.%; K_2O: 0.002–1.94 wt.%. The values reported in gray in Table 2 represent the limit of detection, calculated for the melt inclusions by following Halter *et al.* (2002) and for the host mineral following Pettke *et al.* (2012); element concentrations in these samples are below the calculated limit of detection.

Host phenocryst chemistry

Olivine, clinopyroxene, and orthopyroxene phenocrysts each exhibit less compositional variability than plagioclase. The Mg# (molar [Mg/(Mg+Fe)]) ranges from 60 to 76 for clinopyroxene, from 49 to 69 for orthopyroxene, and from 68 to 81 for olivine. Plagioclase phenocrysts cover a larger compositional range, from anorthite rich (e.g., $An_{93}Ab_7$; 17mrb24) to moderately albite rich (e.g., $An_{35}Ab_{62}Or_3$; 16mrb16) (Table 1). The EPMA data for plagioclase phenocrysts revealed normal (i.e., higher Ca in the core than the rim of the crystal), reverse (i.e., lower Ca in the core than the rim of the crystal), and oscillatory zoning in phenocrysts from all eruptive centers (Robertson 2011).

Melt inclusion chemistry

The chemical compositions of melt inclusions range from picrobasalt to rhyolite (Table 2, Fig. 4). Whole-rock and melt inclusion total alkalis versus SiO_2 concentrations for each sample (Fig. 4) reveal a subalkaline composition as is typical for subduction zone settings and indicate that whole-rock compositions usually lie in between the compositions of individual melt inclusions from the same sample. Silica variations among melt inclusions from one rock sample are as small as 10 wt.% (e.g., sample CM-113) to as large as 24 wt.% (e.g., sample CM-8a). Major element concentrations of melt inclusions from all samples have larger compositional ranges than the range of all whole-rock values, consistent with other melt inclusion studies (e.g., Kent *et al.* 2010). Exceptions are samples M1-02-08, CM-5 and CM-113 for which almost all analyzed individual melt inclusions are more silicic than bulk rock values.

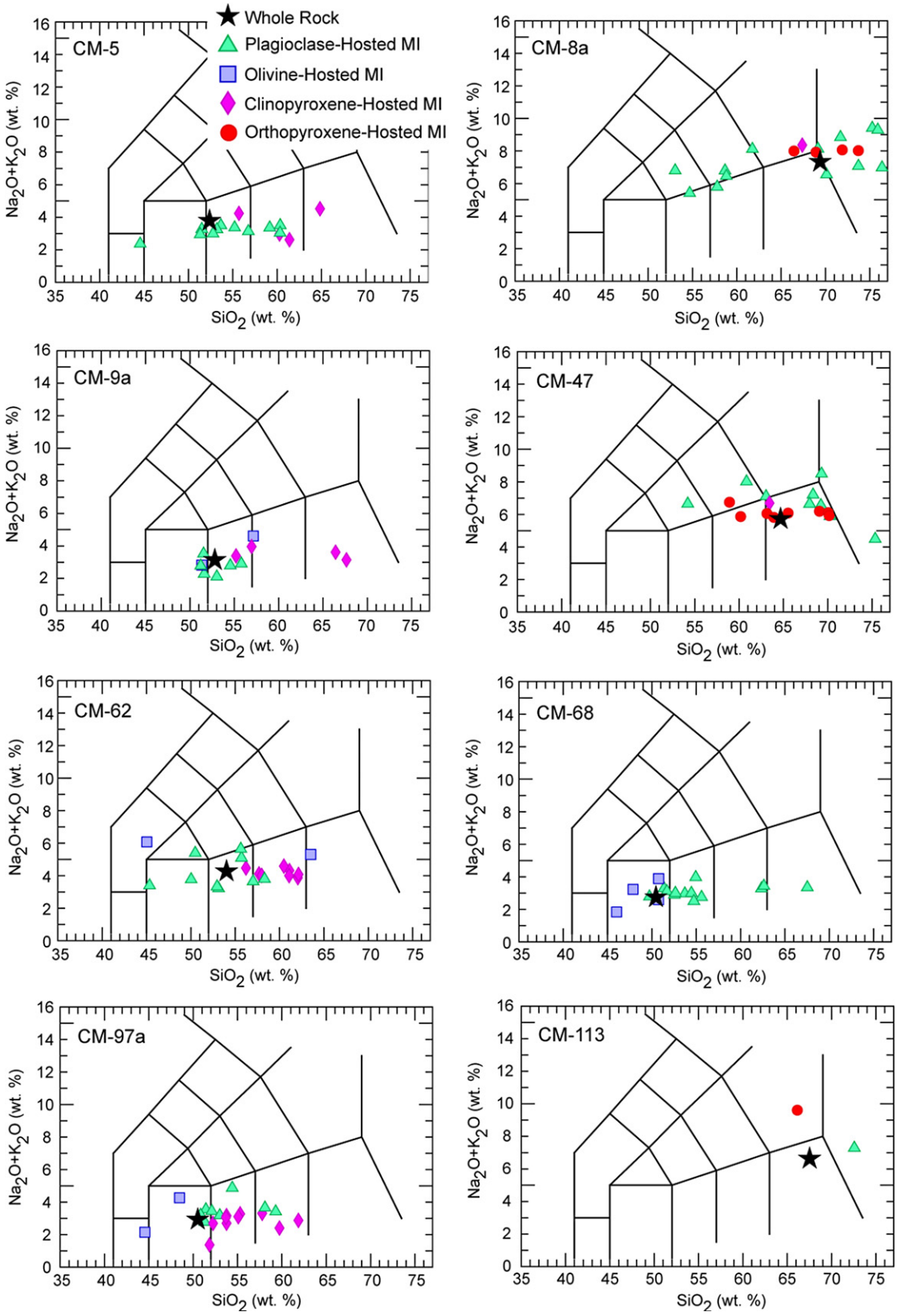

Fig. 4. Le Bas (Le Bas *et al.* 1986) diagram classifying whole-rock and melt inclusion samples by total alkalis and silica. Fields plotted on each diagram are explained in the bottom right panel.

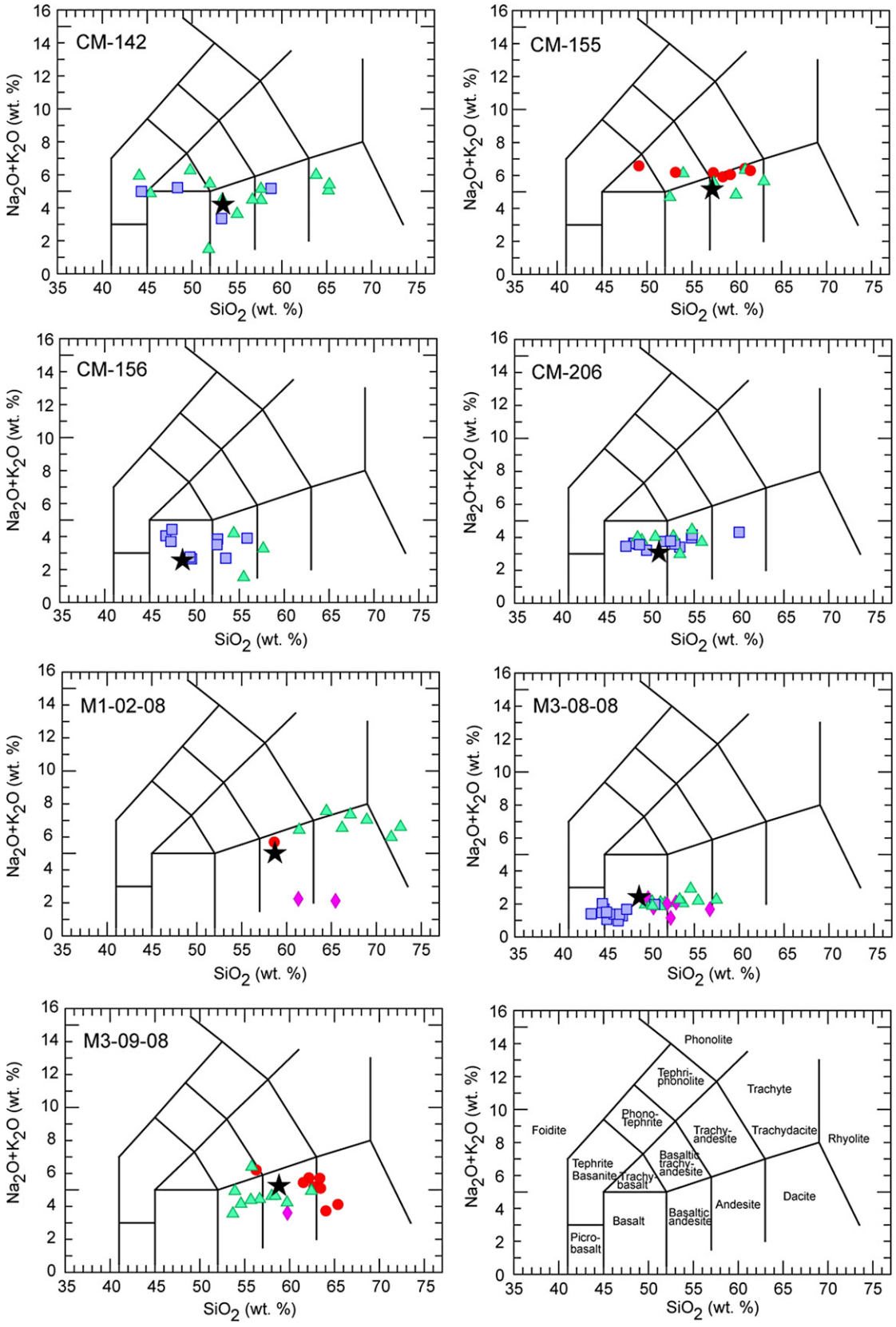

Fig. 4b. Continued.

Melt inclusion major and trace element compositions are broadly similar for all eruptive centers (Mutnovsky I-IV). Melt inclusion trace element patterns are very similar to their whole-rock trace element patterns, showing a typical subduction signature. Melt inclusions are enriched in the large ion lithophile elements (LILE) and, to a lesser degree, in the light rare earth elements (LREE), and, are depleted in the high field strength elements (HFSE), notably Nb (Fig. 5). When considering the incompatible trace element ratios Rb versus Ba, Rb versus La, Rb versus Sr, and Zr versus Th in samples CM-8a and CM-62, whole-rock values plot close to mixing lines between the most enriched and depleted (for the trace element of interest) melt inclusion values (Fig. 6). Simple linear mixing lines were calculated by choosing end points for the mixing lines that best represent the extremes of the melt inclusion population for each sample. Note that Sr is the only element that is somewhat compatible because of the presence of plagioclase in the system. There are some melt inclusions that plot outside the general trend of the melt inclusion population and do not conform to a mixing trend. The two samples portrayed in Fig. 6 are generally representative of the entire sample population.

Melt inclusions by host mineral

The melt inclusion data indicate that different phenocryst host minerals trapped different melt inclusion compositions (Figs 4–8). Plagioclase is the most prevalent phenocryst phase at Mutnovsky, occurring in all samples, and it has the highest number of analyzed melt inclusions and the widest range of melt inclusion compositions. When compared with whole-rock compositions, clinopyroxene, orthopyroxene, and plagioclase, all contain melt inclusions that

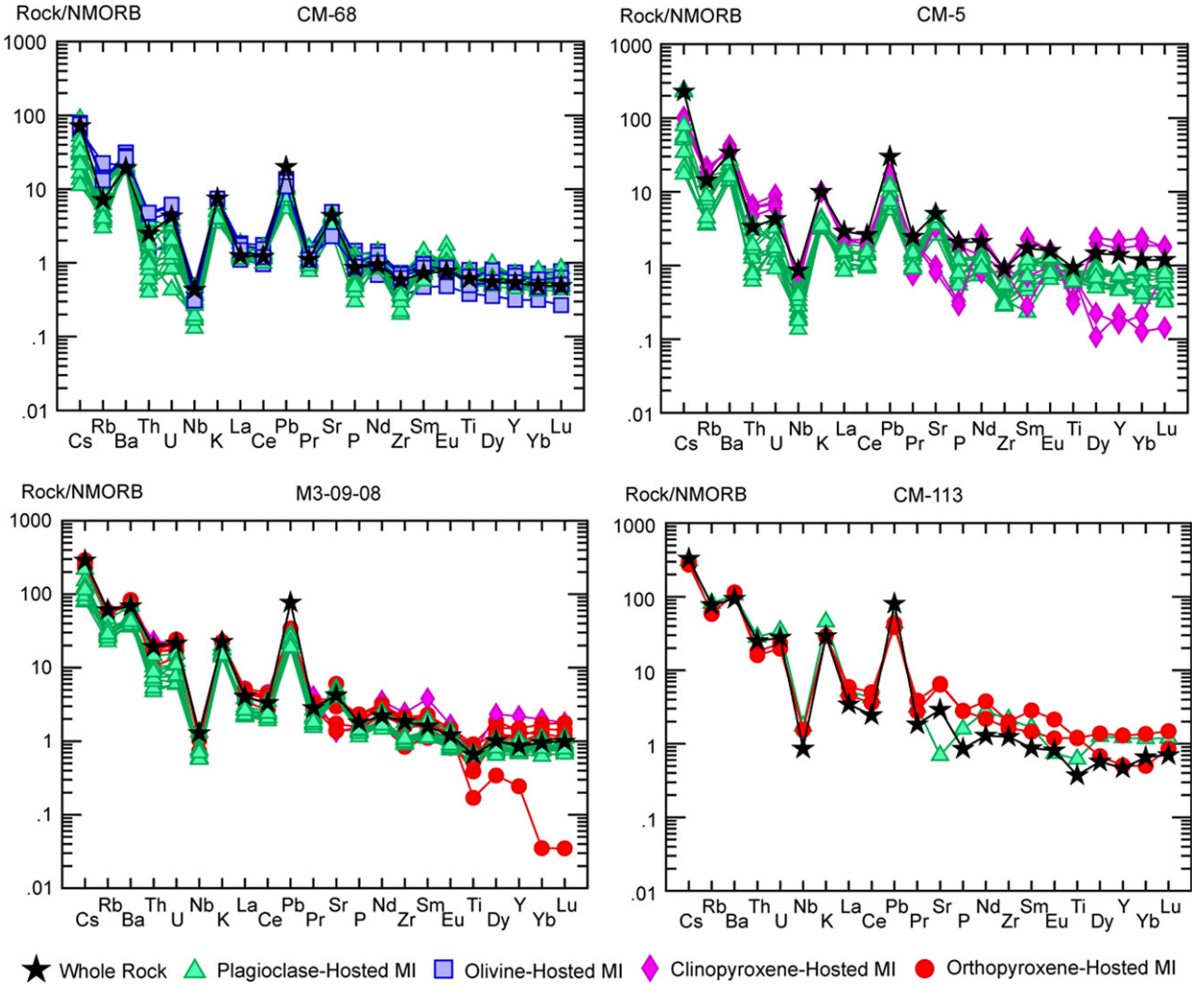

Fig. 5. Trace element abundances normalized to normal mid-ocean ridge basalt (Sun & McDonough 1989) for four representative samples, one from each eruptive center and of each whole-rock type. CM-68 is a basalt from Mutnovsky IV, CM-5 is a basaltic andesite from Mutnovsky I, M3-09-08 is an andesite from Mutnovsky III, and CM-113 is a dacite from Mutnovsky II.

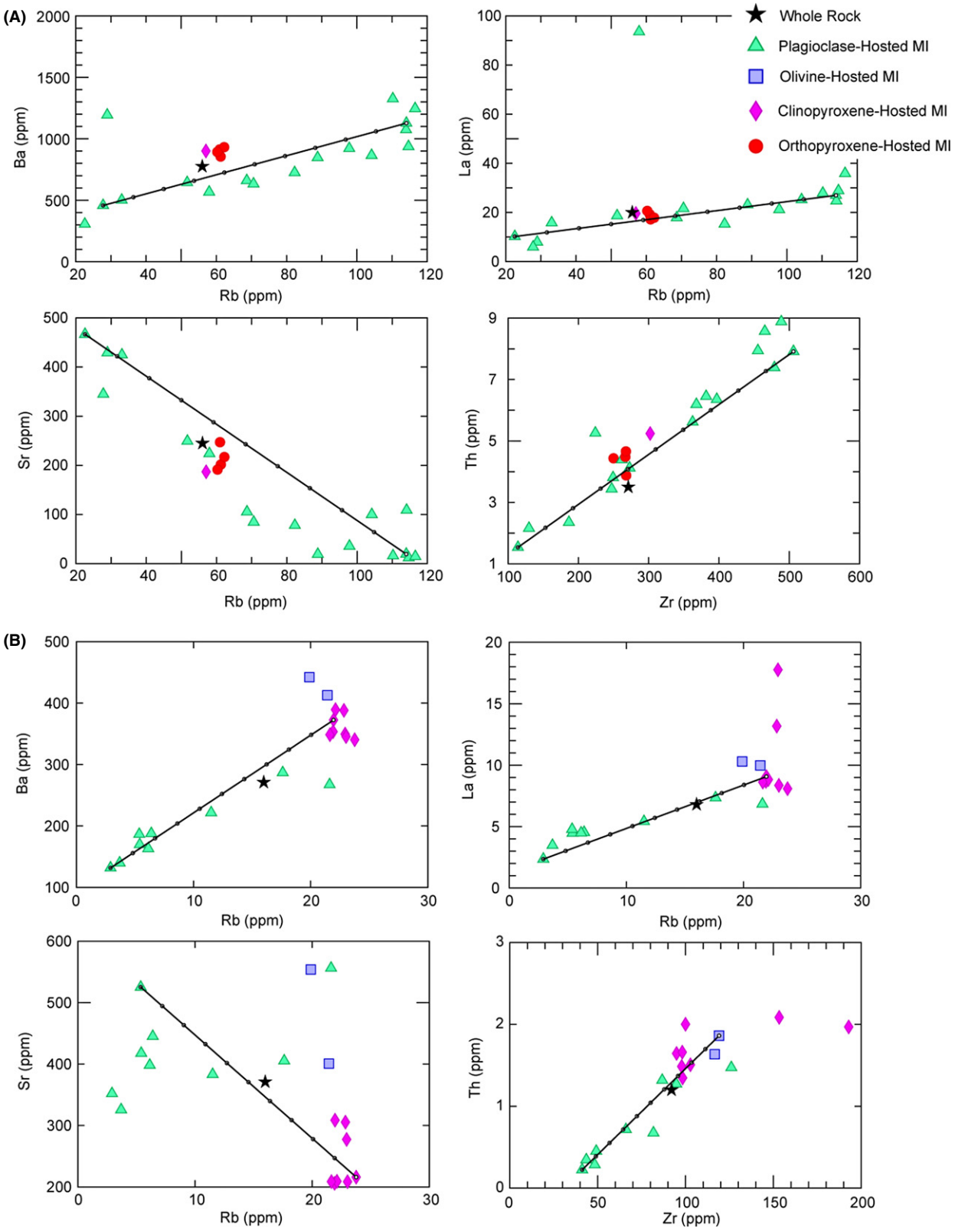

Fig. 6. Trace element plots for melt inclusions from two representative samples, CM-8a (A) and CM-62 (B). Mixing lines are plotted that were calculated by choosing end points that best represent the extremes of the melt inclusion population for each sample between the most and least evolved melt inclusions; each dot along the mixing line represents 10% mixing increments.

span the compositional range of the whole rocks and extend to more silica-rich compositions (Fig. 7). Olivine-hosted melt inclusions have compositions that overlap the composition of the whole rock and also extend to more silica-poor compositions (Fig. 7).

The average concentration of SiO_2 among melt inclusions for each host mineral is compared in Fig. 8 with the whole-rock SiO_2 value for each sample. Plagioclase-hosted melt inclusions have the highest SiO_2 values, while olivine-hosted melt inclusions have the lowest SiO_2 values. Samples CM-206, CM-9a, CM-156, CM-113, and CM-5 have whole-rock SiO_2 concentrations that are lower than all of the average melt inclusion SiO_2 concentrations per host phenocryst.

One important question in any melt inclusion study is whether or not the measured variability of melt inclusion compositions reflects postentrapment crystallization. We assessed this possibility for each melt inclusion – host phenocryst pair. For plagioclase, the compositions of melt inclusions vary as follows: Al_2O_3: 7.42–24.77 wt.%; MgO: 0.33–8.33 wt.%; FeO_T: 2.77–16.17 wt.%; SiO_2: 48.7–75.25 wt.%; K_2O: 0.19–5.42 wt.%; CaO: 0.45–16.49 wt.%; Na_2O: 0.96–6.06 wt.%; and TiO_2: 0.46–1.93 wt.%. We evaluated whether or not the range of measured concentrations of plagioclase-hosted melt inclusions reflect postentrapment modification by assessing the correlation between highly incompatible elements in plagioclase (e.g., Fe, Ti, Mg, Sc, Cr, Mn, Y; Aigner-Torres 2003) and the Al_2O_3

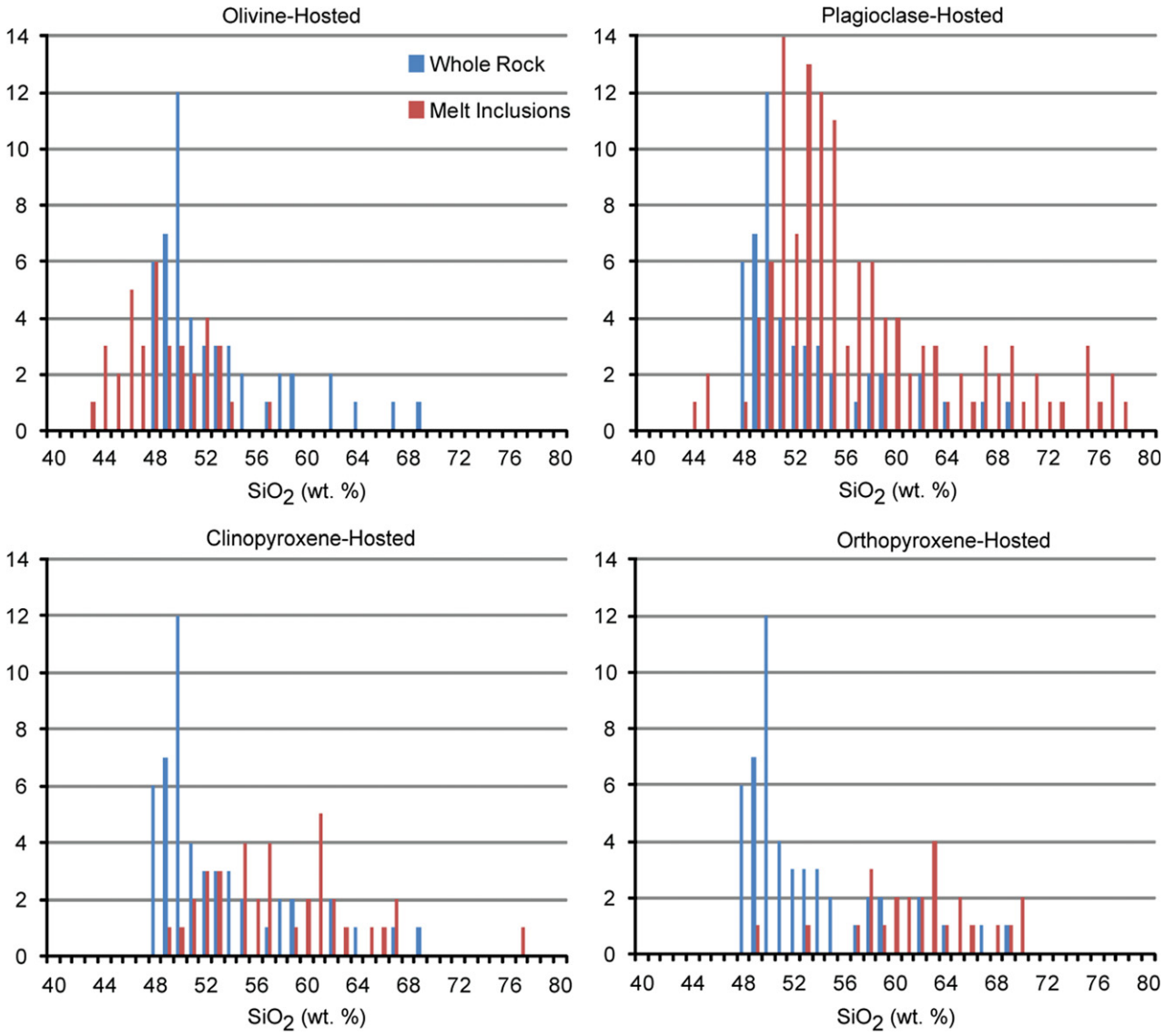

Fig. 7. Frequency diagrams showing the number of melt inclusions and whole rocks with different SiO_2 compositions, by melt inclusion host phenocryst. The whole-rock values plotted include all 50 samples reported in Robertson (2011) and not just the rocks with melt inclusions analyses.

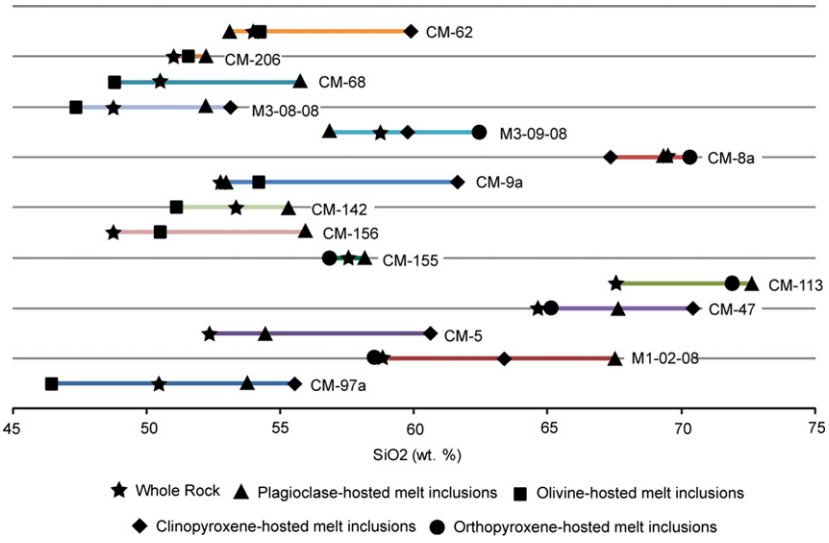

Fig. 8. Average SiO_2 values for melt inclusions in every host mineral, compared with whole-rock values, for every sample. Each line represents the range in average values for a given sample. Standard deviations for SiO_2 values in melt inclusions from each host mineral are as follows: plagioclase: average 1.03, range 0.21–3.65 wt.%; olivine: SiO_2: average 1.02, range 0.32–3.24 wt.%; cpx: average 1.49, range 0.40–4.10 wt.%; opx: 1.78, range 0.63–4.55 wt.%. Samples where the whole-rock composition is less evolved than all the average melt inclusion data provide unambiguous evidence for addition of a basaltic magma just before eruption. Hence, magma mixing appears likely to trigger volcanic eruptions.

content of the melt inclusion. Figure 9 illustrates this relationship for the concentrations of FeO, MgO, TiO_2, and Y in plagioclase-hosted melt inclusions and the Al_2O_3 concentration of the melt inclusion. Postentrapment crystallization should increase the concentrations of highly incompatible elements as the concentration of Al_2O_3 in the melt inclusion decreases, which occurs because of the crystallization of plagioclase around the edges of the melt inclusion (Streck & Wacaster 2006). This is not observed for the majority of melt inclusions. Rather, the concentrations of FeO, MgO, TiO_2, and Y predominantly remain relatively constant as a function of Al_2O_3 concentrations of the melt inclusion. We interpret these data to indicate that the measured variability of plagioclase-hosted melt inclusion compositions reflects the actual diversity of melt compositions during the evolution of the Mutnovsky magma system.

Similar observations can be made for cpx-, opx-, and ol-hosted melt inclusions. The compositions of melt inclusions and cpx-, opx-, and ol-host mineral phases consistently yielded calculated values in terms of oxide totals that are 99–102 wt.% and yielded olivine Fe-Mg K_D values within approximately 10% of published values. We interpret these data to indicate that the measured variability of melt inclusions in cpx-, opx-, and ol-hosted melt inclusions likely reflects the compositional variability at the time of entrapment.

DISCUSSION AND INTEPRETATION

Petrographic evidence, field evidence (Fig. 10A), and phenocryst zonation patterns (Robertson 2011) are consistent with magma mixing and mingling throughout the evolution of Mutnovsky igneous activity. Field evidence for magma mingling includes mafic enclaves, interpreted to have chilled margins, found in a more felsic Mutnovsky I host (Fig. 10A). Resorbed and sieve-textured plagioclase phenocrysts are abundant in samples from every eruptive center and for every major rock composition (Fig. 10B). EPMA traverses across plagioclase phenocrysts indicate that plagioclase crystals are commonly zoned (Robertson 2011). Normally zoned and oscillatory-zoned plagioclase phenocrysts are the most common in Mutnovsky samples, and there are some reversely zoned plagioclase phenocrysts. We note that rapid decompression is also a plausible explanation for the observed sieve texture of plagioclase (Nelson & Montana 1992) and that reverse zoning (i.e., Ca-enriched rims on sodic plagioclase) can be caused by decompression-induced resorption of clinopyroxene, which effectively increases the Ca to Na ratio of the melt, or melt devolatilization during ascent. The plagioclase dissolution textures reported by Nelson & Montana (1992) were reproduced by performing fluid absent, isothermal decompression experiments from an initial pressure of 1.2 GPa to final pressures of 1.0, 0.8, and 0.6 GPa. Kadik *et al.* (1989) demonstrated experimentally that clinopyroxene is not a stable phase in high-Al Kamchatkan basalts at pressures > approximately 0.7 GPa. Thus, it seems unlikely that the coarsely sieve-textured plagioclase cores formed by strictly by decompression. Compositional variation among plagioclase crystals may also reflect the effects of decompression-induced volatile saturation and changing H_2O concentration of silicate melts. Crabtree & Lange (2011)

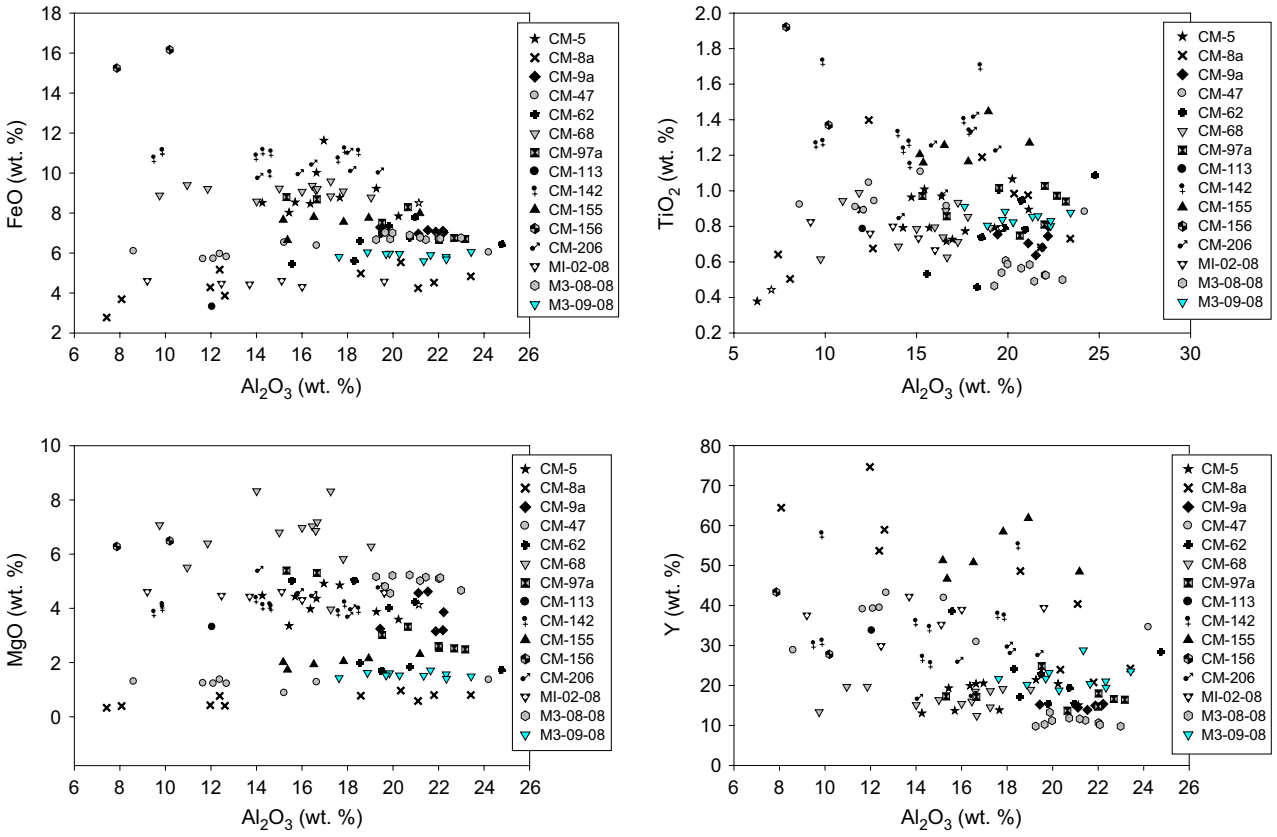

Fig. 9. The concentrations of MgO, FeO, TiO_2, and Y in plagioclase-hosted melt inclusions are plotted against the concentration of Al_2O_3 in the plagioclase host. These elements (i.e., MgO, FeO, TiO_2, and Y) are highly incompatible in plagioclase, and their variation as a function of Al_2O_3 in the plagioclase-hosted melt inclusion indicates that the measured range of melt inclusion compositions trapped in plagioclase crystals reflects the compositional variability of melts at the time of entrapment in plagioclase.

and Frey & Lange (2011) investigated the compositional variability of plagioclase grains from andesites and dacites erupted at the western Mexico volcanic belt and suggested that the effect of higher H_2O concentrations of silicate melt is to reduce the activity of CaO relative to $NaO_{0.5}$, favoring higher sodium contents of crystallizing plagioclase. If the silicate melt reaches volatile saturation during ascent, the loss of dissolved H_2O from the melt increases the activity of CaO and increases the Ca/Na ratio of crystallizing plagioclase. The petrographic observations of dusty, zoned plagioclase in the current study (Fig. 10B), both normal and reverse chemical zoning of individual plagioclase crystals, and the compositions of plagioclase-hosted melt inclusion, seem most consistent with magma mixing and likely also record variation in the pre-eruptive H_2O concentrations and decompression-induced degassing, as the causes of the observed variation of plagioclase compositions and morphologies. A detailed evaluation of plagioclase phenocrysts was not considered during this study.

The measured compositional heterogeneity of erupted rocks at Mutnovsky was interpreted by Robertson (2011) to reflect different amounts and variable depths of partial melting in the subarc mantle source followed by closed system fractional crystallization. The new melt inclusion data presented here allow us to extend that study and further investigate the cause(s) of the variability of whole-rock geochemical compositions. The variability of melt inclusion compositions among different host minerals provides information on the pre-eruptive melt compositions as well as crystallization history. Each host mineral (i.e., olivine, clinopyroxene, orthopyroxene, plagioclase) contains a different range of melt inclusion compositions (Fig. 7), while individual phenocrysts have rather uniform melt inclusion compositions. Notably, some individual plagioclase phenocrysts contain multiple melt inclusions that vary in melt SiO_2 content by 6–15 wt.%. This variability likely reflects the prevalence of plagioclase to crystallize continually throughout the fractionation history of subvolcanic magma reservoirs and during eruption. Such an extended period of crystallization for plagioclase predicts that plagioclase should trap a wider range of melt compositions relative to other phases that are not stable throughout the entire crystallization sequence.

Fig. 10. Visual evidence consistent with magma mixing observed in the field (A) and in thin section (B). Part (A) shows mafic enclaves with chilled margins hosted in a more felsic matrix. Part (B) shows abundant sieve-textured plagioclase.

We highlight that there is no correlation between host phenocryst size and the range of melt inclusion compositions. Individual plagioclase phenocrysts with large ranges of melt inclusion compositions range in size from approximately 200 to 2000 μm diameter. Individual olivine and pyroxene phenocrysts have similar size ranges, but do not trap as large of a range in melt inclusion compositions (e.g., Fig. 6). The ranges of melt inclusion SiO_2 values as a function of different host phenocryst sizes are shown in Fig. 11. If fractional crystallization was the only differentiation process responsible for the observed whole-rock chemical variability, this predicts that small phenocrysts, which likely represent late stage crystallization, would have trapped the most chemically evolved (i.e., higher SiO_2) melts. However, for the Mutnovsky samples, small (≤250 μm) phenocrysts also trapped a range of melt inclusion compositions, which vary from basalt to rhyolite (Fig. 11).

If the small phenocrysts represent crystals that nucleated and grew closer to the time of eruption, then this observation (i.e., size versus. composition variability) suggests three possibilities. First, that magma mixing caused some of the compositional heterogeneity of the whole rocks. In this scenario, it is plausible that the small host phenocrysts crystallized and trapped different melt inclusion compositions in individual, separate magma batches that were later mixed together to produce the erupted whole-rock compositions. Second, that convection within an evolving and compositionally zoned magma chamber mechanically mixed together less-evolved and more evolved magma zones. In this scenario, the bulk magma chamber may have differentiated primarily by fractional crystallization (consistent with the whole-rock data presented in Robertson 2011), and convective mixing of compositionally variable portions of the chamber resulted in the textural and compositional variability of the erupted rocks. Third, there may have been periodic injection of mafic magma into a compositionally evolving magma that was differentiating primarily by fractional crystallization. This process could cause convection, on at undefined scale, and, if this also stimulates eruption, is predicted to yield 'mixed' compositions of erupted rocks, consistent with melt inclusion evidence in this study.

Single melt inclusion outliers in plagioclase-hosted melt inclusions in sample CM-142 can be explained by differences among melt inclusion assemblages. Melt inclusions 23mrc11-14 were all trapped in one plagioclase phenocryst. The inclusions 23mrc11-13 were part of one melt inclusion assemblage trapped in the outer portion of the plagioclase phenocryst (i.e., closer to the crystal rim), and inclusion 23mrc14 was trapped near the core of the plagioclase phenocryst. The measured concentrations of SiO_2 in inclusions 23mrc11-13 are lower than inclusion 23mrc14. This finding is consistent with reverse zoning with respect to trapped melt inclusion compositions. Another plagioclase phenocryst in the same thin section contained melt inclusions 23mrc18-19. In that phenocryst, the melt inclusion 23mrc18 was part of a low SiO_2 melt inclusion assemblage located in the core of the phenocryst and melt inclusion 23mrc19 was part of a high SiO_2 melt inclusion assemblage located in the rim of the phenocryst. These compositional observations, that is, lower SiO_2 in melt inclusions in the crystal core and higher SiO_2 in melt inclusions in the crystal rim, are consistent with fractional crystallization trends.

Halter *et al.* (2004a) suggested that different melt inclusion compositions trapped by different host minerals indicates that the phenocrysts did not crystallize from a single melt that evolved via fractional crystallization. They suggested that such a scenario requires compositionally distinct, separately evolving magmas (crystals + melt) where melt was trapped as melt inclusions by the different phenocryst phases. Accordingly, the measured variability of SiO_2 concentrations in melt inclusions among different host

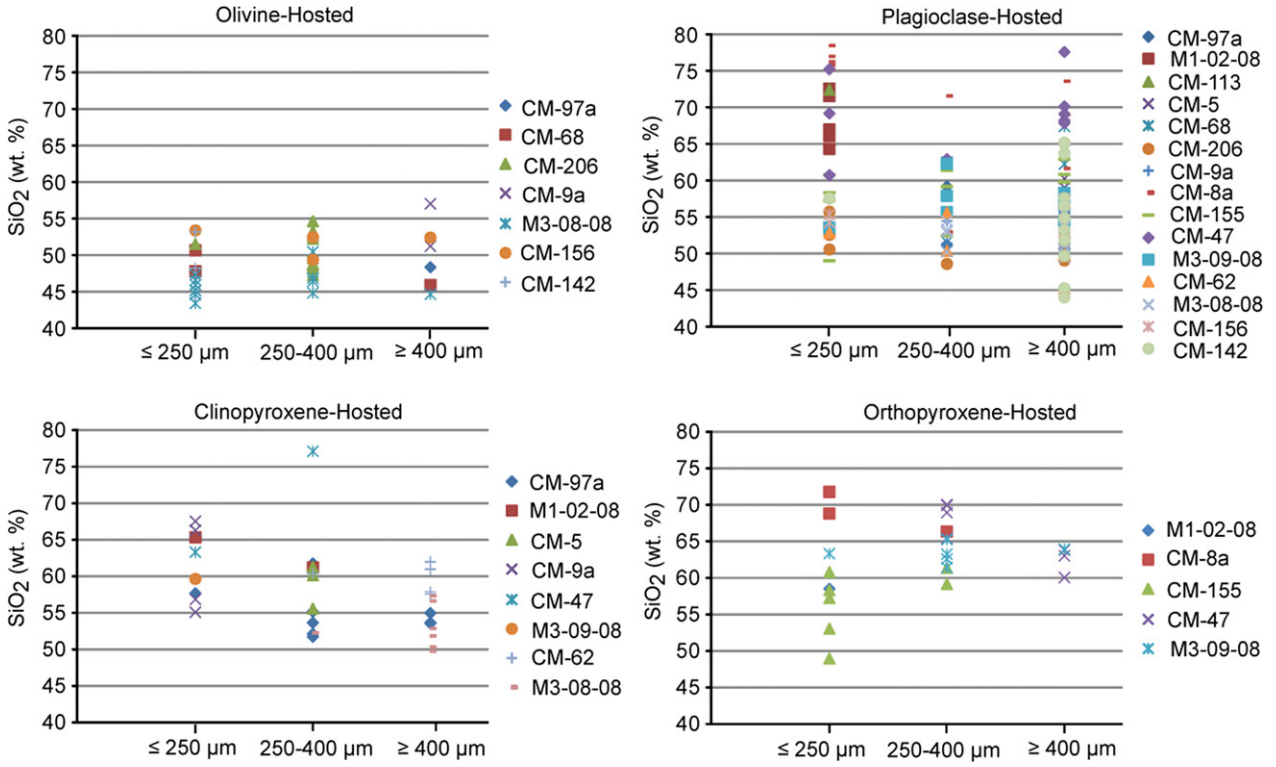

Fig. 11. Melt inclusion SiO_2 compositions by host phenocryst size. Host phenocryst sizes are split into categories small (1; ≤250 μm), medium (2; 250–400 μm), and large (3; ≥400 μm).

minerals helps constrain the compositions and evolutionary stages of magmas involved in the formation of Mutnovsky eruptive centers. The melt inclusions hosted in plagioclase seem to record both prominent fractional crystallization (i.e., increasing wt.% SiO_2 in melt inclusions trapped from core to rim, 23mrc18-19) and mixing of different magma batches (i.e., decreasing wt.% SiO_2 in melt inclusions from core to rim, 23mrc11-14), data that are consistent with the measured normal and reverse zoning of plagioclase phenocryst compositions (Robertson 2011).

Olivine-hosted melt inclusions tend to have low silica compositions (e.g., Fig. 8), suggesting that olivine was crystallizing as the liquidus phase from a primitive melt composition. Clinopyroxene-hosted melt inclusions contain mostly basaltic through andesitic compositions, indicating that clinopyroxene crystallized from a mafic to intermediate melt. This could be a single melt evolving via fractional crystallization or mixing of multiple magma compositions, similar to magma mixing recorded in plagioclase melt inclusions. Orthopyroxene-hosted melt inclusions predominately contain andesitic and dacitic compositions, indicating that orthopyroxene crystallized from an intermediate to evolved melt.

Geochemical modeling of whole-rock fractional crystallization indicates that a normal fractionation sequence occurred at Mutnovsky, with olivine crystallizing early as the liquidus phase, clinopyroxene and orthopyroxene crystallizing after olivine, and plagioclase crystallizing throughout the crystallization sequence. Trace element fractional crystallization geochemical modeling cannot produce the range of compositions recorded by melt inclusions among all the mineral phases combined. Additional evidence for the primitive nature and early crystallization of olivine and also clinopyroxene is the high Cr content of melt inclusions hosted within those mineral phases (Fig. 12A; Wilson 1989). Chromium is compatible with respect to primitive mantle minerals such as olivine, pyroxene, and spinel, so high (>200 ppm) Cr content in melt inclusions signifies that these minerals have not extensively crystallized prior to entrapment. There is some overlap in the melt inclusion compositions within each host mineral, but because of the prevalence of different average melt inclusion compositions for each host mineral and the trace element modeling results, the data seem consistent with a model wherein different magma batches evolved by fractional crystallization, with subsequent magma mixing occurring during or prior to eruption. A lack of equilibrium among coexisting orthopyroxene and clinopyroxene in some samples, assessed using QUILF (Andersen *et al.* 1993), is consistent with magma mixing for such samples. We propose that this is the result of multiple injections of unique melt aliquots from the same source, evinced by statistically overlapping

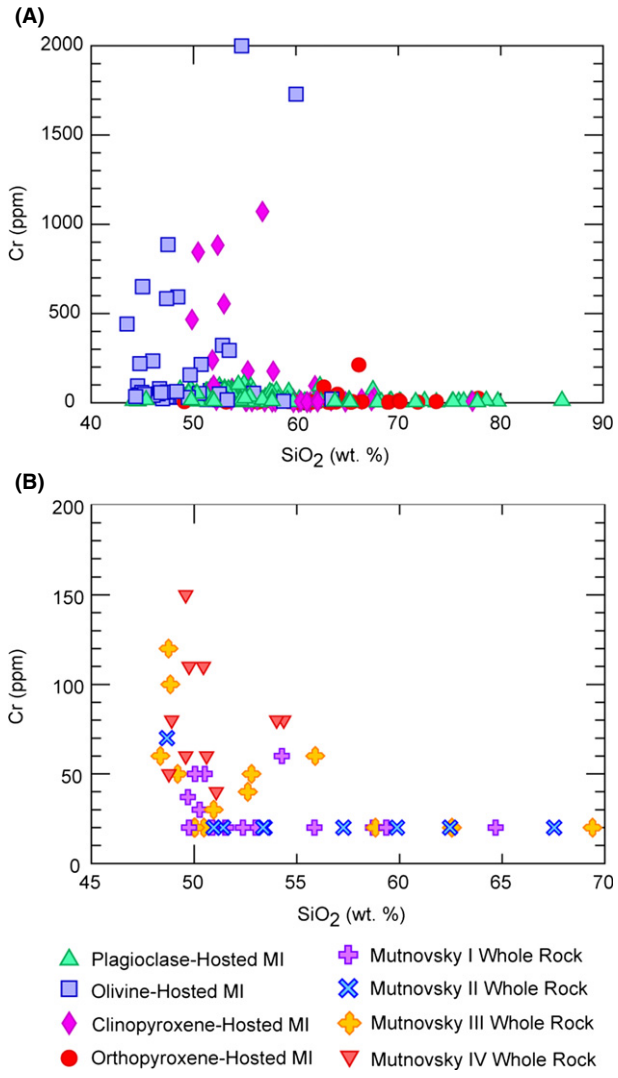

Fig. 12. SiO_2 versus Cr concentrations for melt inclusions hosted by (A) minerals and (B) whole-rock samples from the four eruptive centers. The limit of detection for Cr for each individual melt inclusions ranged from a low of approximately 1 ppm to a high of approximately 27 ppm (Table 2). Thus, the data plotted here indicate that ol- and cpx-hosted melt inclusions trapped the compositionally least evolved melts.

Sr, Nd, and Pb isotopes (Table 1) that evolved separately and not simply by fractional crystallization of one melt, except in the case of intramineral melt variation. We note that low Cr contents of plagioclase-hosted melt inclusions (Table 1) indicate that plagioclase was not a liquidus phase in the deep source magma.

Comparing the melt inclusion total alkalis versus silica data to their host rocks (Fig. 4) further illustrates that the compositions of whole rocks investigated in this study likely represent a mixture of melts. In samples where olivine-hosted melt inclusions are present, these inclusions represent a mafic mixing end member. In all other samples, plagioclase or orthopyroxene inclusions represent a felsic mixing end member. Geochemical modeling of melt inclusion trace element abundances (IgPet: Carr 2002) indicates that the most felsic melt inclusions in each whole-rock sample can be produced by varying degrees (30–70%) of fractional crystallization (including olivine, plagioclase, clinopyroxene, and orthopyroxene) of the most mafic melt inclusions from the same sample. However, fractional crystallization alone cannot explain the entire range of melt inclusion compositions found in one phenocryst type. Therefore, the data seem consistent with discrete aliquots of melt that were trapped as fractional crystallization occurred, prior to magma mixing events.

There are many examples of magma mixing in volcanic systems discovered only after analyzing melt inclusions, such as Mount Hood (Kent *et al.* 2010) and the Farallón Negro Volcanic Complex (Halter *et al.* 2004a), and individual phenocrysts, such as the Fish Canyon Magmatic System (Charlier *et al.* 2007). In the aforementioned volcanic systems, magma mixing was not apparent when looking at large scale, whole-rock data, but became obvious after examining small scale data such as melt inclusions and chemical zoning of individual phenocrysts. These studies all focused on volcanic systems that, at least in terms of the bulk composition of erupted rocks, are largely andesitic (Mount Hood and Farallón Negro) or rhyolitic (Fish Canyon). Mutnovsky is a dominantly basaltic system that preserves evidence consistent with the characteristics of magma mixing described in the aforementioned studies. Magma mixing has been demonstrated in a few basaltic systems including Stromboli volcano (Francalanci *et al.* 1989) and mid-ocean ridge volcanism (Dungan & Rhodes 1978), but it is far less commonly observed than in more intermediate to silicic systems (Izbekov *et al.* 2004; Kent *et al.* 2010). This infrequency of observation should not be interpreted to imply that magma mixing is not potentially an important process in basaltic systems. Perhaps magma mixing is simply less obvious because the mixing inputs are closer in composition to one another, particularly if they have overlapping isotopic compositions (Table 1) as is the case at Mutnovsky. Similar observations were reported by Izbekov *et al.* (2004) for mixing of basalt and andesite prior to the 1996 eruption of Karymsky Volcano, Kamchatka. Those authors used multiple lines of evidence to suggest that injection of basalt magma into an andesite reservoir triggered eruption of a poorly mixed basalt–andesite magma. The earliest eruptions contain evidence for disequilibrium between the basalt and andesite, and progressively younger eruptions contain compositionally equilibrated materials. Several studies reported evidence for magma mixing where the mixed magma was not chemically homogenized at the time of eruption; for example, Unzen, Japan (Nakamura 1995); Dutton, Alaska (Miller *et al.* 1999); and Soufrière Hills (Murphy *et al.* 2000). Izbekov *et al.* (2004) postulated that compositional homogeneity of mixed magmas is favored if, at the time of

mixing, the two magmas have similar temperatures, viscosities, and densities. As the differences in temperature, viscosity, and density of the melts increase, this seemingly prevents efficient magma mixing and should lead to eruption of compositionally heterogeneous material where (inefficient) magma mixing is more obvious.

A model for magma 'chamber' evolution at Mutnovsky

The melt inclusion and whole-rock chemistry data for samples from all eruptive centers at Mutnovsky are consistent with the hypothesis that the erupted rocks represent the crystallized products of multiple aliquots of different magma compositions, possibly from different depths of the shallow-level pre-eruptive plumbing system, that mixed together prior to and/or during eruption. This is similar to the model proposed for other arc volcanoes, for example Mount St. Helens (Blundy & Cashman 2005), where the minimum trapping pressure (determined from H_2O contents of melt inclusions) of melt inclusions from samples from individual eruptions indicate multiple depths of magma storage from a plumbing system that spanned a vertical distance on the order of several km. The melt inclusions from Mutnovsky, as is the case for the whole rocks, are enriched in the fluid mobile LILE and LREE (Fig. 5), a finding that is consistent with fluid-driven melting of the mantle wedge at the base of the Mutnovsky magma plumbing system, as proposed by Duggen *et al.* (2007) based on their interpretation of Sr, Nd, and (double-spike MC-ICP-MS) Pb isotope data. As individual pulses of magma were emplaced into the near-surface environment, each pulse differentiated by fractional crystallization. The addition of new, hot, potentially volatile-rich, less-evolved magma is a plausible eruption trigger (Sparks *et al.* 1977; Venezky & Rutherford 1997; Eichelberger *et al.* 2000; Murphy *et al.* 2000; Kent *et al.* 2010), which could result in the eruption of an apparent single magma that is in reality a composite of formerly discrete, fractionally crystallized magmas. If input of basaltic magma and concomitant mixing did not immediately result in eruption, this could provide time sufficient for resorption of mafic phenocrysts, hence enriching the bulk magma in those components and decreasing the SiO_2 content. This process could obscure the mafic end member portion of the melt record as we found via the absence of mafic melt inclusions in some samples.

CONCLUSIONS

1 Melt inclusion compositions range from low silica (44 wt.%), hosted mainly in olivine, to high silica (75 wt.%), hosted in plagioclase. Multiple melt populations are required to explain the range of melt inclusion compositions present in each of the melt inclusion host phases (olivine, clinopyroxene, orthopyroxene, plagioclase). This suggests that multiple magma batches were present throughout the evolution of the Mutnovsky igneous system.
2 The composition of Mutnovsky melt inclusions is consistent with aqueous fluid-flux melting of the mantle wedge and compositional differentiation via fractional crystallization during ascent. As the magmas ponded in the near-surface subvolcanic environment, they continued to evolve via fractional crystallization to produce the range of melt inclusions compositions (basalt to rhyolite) sampled in this study.
3 Periodic injection of new magma, which had undergone fractional crystallization during ascent, ultimately was likely responsible for driving volcanic eruptions. At present, there are no quantitative constraints on the length of time that elapsed between the input of individual magma pulses, or the specific composition of the pre-existing magma reservoir and the intruding magma. However, we suggest that the lag time between magma emplacement and eruption may have controlled the degree to which erupted materials homogenized. This conclusion is consistent with Izbekov *et al.* (2004) who documented that injection of basalt into andesite magma caused eruption of a mixed magma at Karymsky Volcano, Kamchatka, with the reservoir returning to a homogeneous composition within months of the first eruption.

ACKNOWLEDGEMENTS

We thank Lindsey Clark for her help with pyroxene EPMA analyses and Racheal Johnsen for her help with whole-rock Sr, Nd, and Pb isotope analyses. Tatiana Rychkova, Anatoly Mushinsky, and Denise Honn all provided valuable assistance in the field. This work was supported by the University of Nevada Las Vegas President's Research Award to Simon and Smith, and the University of Nevada Las Vegas President's Graduate Fellowship, the Nevada Stars Graduate Fellowship, and ExxonMobil Scholarship to Robertson. We sincerely appreciate reviews from Pavel Izbekov, one anonymous reviewer, and Editor Craig Manning, all of which significantly improved the manuscript substantively and stylistically.

REFERENCES

Aigner-Torres M (2003) Iron, magnesium and other highly incompatible elements partitioning between plagioclase and basaltic melts. PhD Dissertation, Naturwissenschaften ETH Zürich, Nr. 15026.

Andersen DJ, Lindsley DH, Davidson PM (1993) QUILF: a PASCAL program to assess equilibria among Fe-Mg-Ti oxides, pyroxenes, olivine, and quartz. *Computers in Geosciences*, **19**, 1333–50.

Anderson AT (1976) Magma mixing: petrological process and volcanological tool. *Journal of Volcanology and Geothermal Research*, **1**, 3–33.

Annen C, Blundy JD, Sparks RSJ (2006) The genesis of intermediate and silicic magmas in deep crustal hot zones. *Journal of Petrology*, **47**, 505–39.

Audétat A, Pettke T (2003) The magmatic-hydrothermal evolution of two barren granites: a melt and fluid inclusion study of the Rito del Medio and Canada Pinabete plutons in Northern New Mexico (USA). *Geochimica et Cosmochimica Acta*, **67**, 97–122.

Bacon CR, Bruggman PE, Christiansen RL, Clynne MA, Donnelly-Nolan JM, Hildreth W (1997) Primitive magmas at five cascades volcanic fields: melts from hot, heterogeneous sub-arc mantle. *The Canadian Mineralogist*, **35**, 397–423.

Blundy J, Cashman K (2005) Rapid decompression-driven crystallization recorded by melt inclusions from Mount St. *Helens volcano. Geology*, **33**, 793–6.

Bodnar RJ, Student JJ (2006) Melt inclusions in plutonic rocks: petrography and microthermometry. In: *Melt Inclusions in Plutonic Rocks* Mineralogical Association of Canada Short Course Series (ed Webster JD), 36, pp. 1–25. Mineralogical Association of Canada, Québec.

Bryant JA, Yogodzinski GM, Churikova TG (2010) High-Mg# andesitic lavas of the Shisheisky Complex, Northern Kamchatka: implications for primitive calc-alkaline magmatism. *Contributions to Mineralogy and Petrology*, **161**, 791–810.

Carr MJ (2002) *IGPET Software*. Terra Softa Inc, Somerset, NJ.

Charlier BLA, Bachmann O, Davidson JP, Dungan MA, Morgan DJ (2007) The upper crustal evolution of a large silicic magma body: evidence from crystal-scale Rb-Sr isotopic heterogeneities in the Fish Canyon Magmatic System, Colorado. *Journal of Petrology*, **48**, 1875–94.

Crabtree SM, Lange RA (2011) Complex phenocryst textures and zoning patterns in andesites and dacites: Evidence of degassing-induced rapid crystallization. *Journal of Petrology*, **52**, 3–38.

Danyushevsky LV, McNeill AW, Sobolev AV (2002) Experimental and petrological studies of melt inclusions in phenocrysts from mantle-derived magmas: an overview of techniques, advantages and complications. *Chemical Geology*, **183**, 5–24.

Defant MJ, Drummond MS (1990) Derivation of some modern arc magmas by melting of young subducted lithosphere. *Nature*, **347**, 662–5.

Duggen S, Portnyagin M, Baker J, Ulfbeck D, Hoernle K, Garbe-Schönberg D, Grassineau N (2007) Drastic shift in lava geochemistry in the volcanic-front to rear-arc region of the Southern Kamchatkan subduction zone: evidence for the transition from slab surface dehydration to sediment melting. *Geochimica et Cosmochimica Acta*, **71**, 452–80.

Dungan MA, Rhodes JM (1978) Residual glasses and melt inclusions in basalts from DSDP legs 45 and 46: evidence for magma mixing. *Contributions to Mineralogy and Petrology*, **67**, 417–31.

Eichelberger JC, Chertkoff DG, Dreher ST, Nye CJ (2000) Magmas in collision: rethinking chemical zonation in silicic magmas. *Geology*, **28**, 603–6.

Francalanci L, Manetti P, Peccerillo A (1989) Volcanological and magmatological evolution of Stromboli volcano (Aeolian Islands): the roles of fractional crystallization, magma mixing, crustal contamination and source heterogeneity. *Bulletin of Volcanology*, **51**, 355–78.

Frey HM, Lange RA (2011) Phenocryst complexity in andesites and dacites from the Tequila volcanic field, Mexico: resolving the effects of degassing vs. magma mixing. *Contributions to Mineralogy and Petrology*, **162**, 415–45.

Guillong M, Meier DL, Allan MM, Heinrich CA, Yardley BWD (2008) SILLS: a MATLAB-based program for the reduction of laser ablation ICP-MS data of homogeneous materials and inclusions. In: *Laser Ablation ICP-MS in the Earth Sciences: Current Practices and Outstanding Issues* Mineralogical Association of Canada Short Course Series (ed Sylvester P), **40**, pp. 328–33. Mineralogical Association of Canada, Québec.

Halter WE, Pettke T, Heinrich CA, Rothen-Rutishauser B (2002) Major to trace element analysis of melt inclusions by laser-ablation ICP-MS: methods of quantification. *Chemical Geology*, **183**, 63–86.

Halter WE, Heinrich CA, Pettke T (2004a) Laser-ablation ICP-MS analysis of silicate and sulfide melt inclusions in an andesitic complex II: evidence for magma mixing and magma chamber evolution. *Contributions to Mineralogy and Petrology*, **147**, 397–412.

Halter WE, Pettke T, Heinrich CA (2004b) Laser-ablation ICP-MS analysis of silicate and sulfide melt inclusions in an andesitic complex I: analytical approach and data evaluation. *Contributions to Mineralogy and Petrology*, **147**, 385–96.

Heinrich CA, Pettke T, Halter WE, Aigner-Torres M, Audétat A, Gunther D, Hattendorf B, Bleiner D, Guillong M, Horn I (2003) Quantitative multi-element analysis of minerals, fluid and melt inclusions by laser-ablation inductively-coupled-plasma mass spectrometry. *Geochimica et Cosmochimica Acta*, **67**, 3473–97.

Hildreth W, Moorbath S (1988) Crustal contributions to arc magmatism in the Andes of central Chile. *Contributions to Mineralogy and Petrology*, **98**, 455–89.

Izbekov PE, Eichelberger JC, Ivanov BV (2004) The 1996 eruption of Karymsky Volcano, Kamchatka: Historical record of basaltic replenishment of andesite reservoir. *Journal of Petrology*, **45**, 2325–45.

Kadik AA, Rozenkhauer M, Lukanin OA (1989) Experimental study of effect of pressure on crystallization of high-Mg and high-Al basalts of Kamchatka. *Geochemistry*, **12**, 1748–62.

Kay RW (1978) Aleutian magnesian andesites: melts from subducted Pacific crust. *Journal of Volcanology and Geothermal Research*, **4**, 117–32.

Kent AJR (2010) Melt inclusions in basaltic and related volcanic rocks. *Reviews in Mineralogy and Geochemistry*, **69**, 273–332.

Kent AJR, Darr C, Koleszar AM, Salisbury MJ, Cooper KM (2010) Preferential eruption of andesitic magmas through recharge filtering. *Nature Geoscience*, **3**, 631–6.

Le Bas MJ, Le Maitre RW, Streckeisen A, Zanettin B (1986) A chemical classification of volcanic rocks based on the total alkali-silica diagram. *Journal of Petrology*, **27**, 745–50.

Leach AM, Hieftje GM (2000) Methods for shot-to-shot normalization in laser ablation with an inductively coupled plasma time-of-flight mass spectrometer. *Journal of Analytical Atomic Spectrometry*, **15**, 1121–4.

Leeman WP (1983) The influence of crustal structure on subduction-related magmas. *Journal of Volcanology and Geothermal Research*, **87**, 561–88.

Manning CE (2004) The chemistry of subduction-zone fluids. *Earth and Planetary Science Letters*, **223**, 1–16.

Métrich N, Wallace PJ (2008) Volatile abundances in basaltic magmas and their degassing paths tracked by melt inclusions. In: *Minerals, Inclusions and Volcanic Processes* . Reviews in Mineralogy and Geochemistry (eds Putirka KD, Tepley FJ), **69**,

pp. 363–402. Mineralogical Society of America, Geochemical Society, USA.
Miller TP, Chertkoff DG, Eichelberger JC, Coombs ML (1999) Mount Dutton Volcano, Alaska: Aleutian Arc analog to Unzen Volcano, Japan. *Journal of Volcanology and Geothermal Research*, **89**, 275–301.
Moore GW, Bogdanov NA, Drummond KJ, Golovchenko X, Larson RL, Pitman WC III, Rinehart WA, Siebert L, Simkin T, Tilman SM, Uyeda S (1992) Plate-tectonic map of the Circum-Pacific Region, Arctic Sheet, in Circum-Pacific Map Series, pp. 20, United States Geological Survey.
Murphy MD, Sparks RSJ, Barclay J, Carroll MR, Brewer TS (2000) Remobilization of andesite magma by intrusion of mafic magma at the Soufriere Hills Volcano, Montserrat, West Indies. *Journal of Petrology*, **41**, 21–42.
Nakamura M (1995) Continuous mixing of crystal much and replenished magma in the ongoing Unzen eruption. *Geology*, **23**, 807–10.
Nelson ST, Montana A (1992) Sieve-textured plagioclase in volcanic rocks produced by rapid decompression. *American Mineralogist*, **77**, 1242–9.
Pettke T (2006) In situ laser-ablation ICP-MS analysis of melt inclusions and prospects for constraining subduction zone magmatism. In: *Melt Inclusions in Plutonic Rocks. Contributions to Mineralogy and Petrology* (eds Webster JD), **36**, pp. 51–80. Mineralogical Association of Canada, Québec.
Pettke T, Halter WE, Webster JD, Aigner-Torres M, Heinrich CA (2004) Accurate quantification of melt inclusion chemistry by LA-ICP-MS: a comparison with EMP and SIMS and advantages and possible limitations of these methods. *Lithos*, **78**, 333–61.
Pettke T, Oberli F, Audétat A, Guillong M, Simon AC, Hanley JJ, Klemm LM (2012) Recent developments in element concentration and isotope ratio analysis of individual fluid inclusions by laser ablation single and multiple collector ICP-MS. *Ore Geology Reviews*, **44**, 10–38.
Plank TP, Langmuir CH (1988) An evaluation of the global variations in the major element chemistry of arc basalts. *Earth and Planetary Science Letters*, **90**, 349–70.
Putirka KD, Tepley F.J III. (2008) Minerals, inclusions and volcanic processes. *Reviews in Mineralogy and Geochemistry*, **69**, 1–8.
Robertson K (2011) Magma chamber processes at Mutnovsky Volcano, Kamchatka. University of Nevada Las Vegas, PhD Dissertation, 336 pp. Available online: http://digitalscholarship.unlv.edu/thesesdissertations/1378/
Schiano P (2003) Primitive mantle magmas recorded as silicate melt inclusions in igneous minerals. *Earth-Science Reviews*, **63**, 121–44.
Selyangin OB (1993) Mutnovsky Volcano, Kamchatka: new evidence on structure, evolution, and future activity. *Volcanology and Seismology*, **15**, 17–38.
Selyangin OB (2009) *Wonderful World of Mutnovsky and Gorely Volcanoes: Volcanologic and Travelers Guide*. Novaja Kniga, Petropavlovsk-Kamchatsky.
Sparks SRJ, Sigurdsson H, Wilson L (1977) Magma mixing—mechanism for triggering acid explosive eruptions. *Nature*, **267**, 315–8.
Streck MJ, Wacaster S (2006) Plagioclase and pyroxene hosted melt inclusions in basaltic andesites of the current eruption of Arenal volcano, Costa Rica. *Journal of Volcanology and Geothermal Research*., **157**, 236–53.
Sun SS, McDonough WF (1989) Chemical and isotopic systematic of oceanic basalts: implications for mantle compositions and processes. In: *Magmatism in the Ocean Basins* (eds Saunders AD, Norry MJ), **42**, pp. 313–345. Geological Society of London, Bath.
Ulmer P (1989) The dependence of the Fe^{2+}-Mg cation-partitioning between olivine and basaltic liquid on pressure, temperature and composition—an experimental-study to 30 k bars. *Contributions to Mineralogy and Petrology*, **101**, 261–73.
Venezky DY, Rutherford MJ (1997) Preeruption conditions and timing of dacite-andesite magma mixing in the 2.2 ka eruption at Mount Rainier. *Journal of Geophysical Research – Solid Earth*, **102**, 20069–86.
Wallace PJ (2005) Volatiles in subduction zone magmas: concentrations and fluxes based on melt inclusion and volcanic gas data. *Journal of Volcanology and Geothermal Research*, **140**, 217–40.
Wilson M (1989) *Igneous Petrogenesis: A Global Tectonic Approach*. Unwin Hyman, London, Boston.
Yogodzinski GM, Kay RW, Volynets ON, Koloskov AV, Kay SM (1995) Magnesian andesite in the Western Komandorsky region: Implications for slab melting and processes in the mantle wedge. *GSA Bulletin*, **107**, 505–19.
Zajacz Z, Halter W (2007) LA-ICP-MS analyses of silicate melt inclusions in co-precipitated minerals: quantification, data analysis and mineral/melt partitioning. *Geochimica et Cosmochimica Acta*, **71**, 1021–40.

SUPPORTING INFORMATION

Additional Supporting Information may be found in the online version of this article:

Table S1. Bulk rock, melt inclusion and host mineral element concentrations.

GEOFLUIDS

Volume 13, Number 4, November 2013
ISSN 1468-8115

CONTENTS

WILEY
Blackwell

Geofluids* is abstracted/indexed in *Chemical Abstracts

This journal is available online at Wiley Online Library.
Visit onlinelibrary.wiley.com to search the articles and register for table of contents and e-mail alerts.